A compressed sensing approach for resolution improvement in fiber-bundle based endomicroscopy

John P. Dumas, Muhammad A. Lodhi, Waheed U. Bajwa, Mark C. Pierce

John P. Dumas, Muhammad A. Lodhi, Waheed U. Bajwa, Mark C. Pierce, "A compressed sensing approach for resolution improvement in fiber-bundle based endomicroscopy," Proc. SPIE 10470, Endoscopic Microscopy XIII, 1047012 (14 February 2018); doi: 10.1117/12.2286360

SPIE.

Event: SPIE BiOS, 2018, San Francisco, California, United States

A compressed sensing approach for resolution improvement in fiber-bundle based endomicroscopy

John P. Dumas[a], Muhammad A. Lodhi[b], Waheed U. Bajwa[b], Mark C. Pierce*[a]
[a]Rutgers, The State Univ. of New Jersey, Dept. of Biomedical Engineering,
599 Taylor Road, Piscataway, NJ, USA 08854
[b]Rutgers, The State Univ. of New Jersey, Dept. of Electrical and Computer Engineering,
94 Brett Road, Piscataway, NJ, USA 08854

ABSTRACT

Endomicroscopy techniques such as confocal, multi-photon, and wide-field imaging have all been demonstrated using coherent fiber-optic imaging bundles. While the narrow diameter and flexibility of fiber bundles is clinically advantageous, the number of resolvable points in an image is conventionally limited to the number of individual fibers within the bundle. We are introducing concepts from the compressed sensing (CS) field to fiber bundle based endomicroscopy, to allow images to be recovered with more resolvable points than fibers in the bundle. The distal face of the fiber bundle is treated as a low-resolution sensor with circular pixels (fibers) arranged in a hexagonal lattice. A spatial light modulator is located conjugate to the object and distal face, applying multiple high resolution masks to the intermediate image prior to propagation through the bundle. We acquire images of the proximal end of the bundle for each (known) mask pattern and then apply CS inversion algorithms to recover a single high-resolution image. We first developed a theoretical forward model describing image formation through the mask and fiber bundle. We then imaged objects through a rigid fiber bundle and demonstrate that our CS endomicroscopy architecture can recover intra-fiber details while filling inter-fiber regions with interpolation. Finally, we examine the relationship between reconstruction quality and the ratio of the number of mask elements to the number of fiber cores, finding that images could be generated with approximately 28,900 resolvable points for a 1,000 fiber region in our platform.

Keywords: Compressive sensing, computational imaging, endomicroscopy.

1. INTRODUCTION

Endoscopic imaging can provide real-time visualization of tissue using coherent fiber optic bundles to transmit images, where each individual fiber in the bundle transmits a single pixel of information. The small diameter and flexibility of these bundles allow for excellent tissue access to facilitate minimally invasive imaging, but manufacturing constraints make it technically challenging to fabricate densely-packed high-resolution bundles. Typical fiber densities are limited to around 30,000 fibers in a 0.72 mm diameter bundle, restricting images to the same number of resolvable points. This usually results in a trade-off between resolution and field of view (FOV) for any given fiber bundle. Consequently, fiber bundles have two fundamental limitations: (1) the number of resolvable points is limited to the number of individual fibers in the bundle, and (2) packing circular fibers together into a bundle results in blank inter-fiber regions, or gaps in the image where tissue regions are not imaged. As a result, images captured through a fiber bundle have significantly lower image quality due to pixilation and discontinuity than images taken without the bundle (Figure 1).

The clinical demand for minimally invasive imaging that provides sub-cellular resolution over a large FOV has led to the proposal of several approaches for improving image quality in fiber-bundle-based endoscopes. One category of approaches use spatial compounding of many shifted images to eliminate pixilation artifacts, with mechanical[1,2], spectral[3], or random transverse[4] shifting techniques. Another category of approaches use the complex speckle pattern produced by mode mixing among individual fiber cores to generate pixilation-free images through fiber bundles[5–8]. Both speckle correlation and image compounding approaches have shown that by recovering information from locations in the inter-fiber gaps, it is possible to achieve resolution better than that dictated by the inter-fiber spacing. However, both approaches are still limited by the total number of fiber cores in the imaging bundle. Recently, reports have presented speckle correlation techniques to overcome the limited number of fiber cores[9,10], but challenges such as large fiber diameter[9] and practical light collection methods[9,10] are hurdles that have yet to be addressed.

*mark.pierce@rutgers.edu; phone 1 848 445-6570; fax 1 732 445-3753

Endoscopic Microscopy XIII, edited by Guillermo J. Tearney, Thomas D. Wang, Melissa J. Suter, Proc. of SPIE
Vol. 10470, 1047012 · © 2018 SPIE · CCC code: 1605-7422/18/$18 · doi: 10.1117/12.2286360

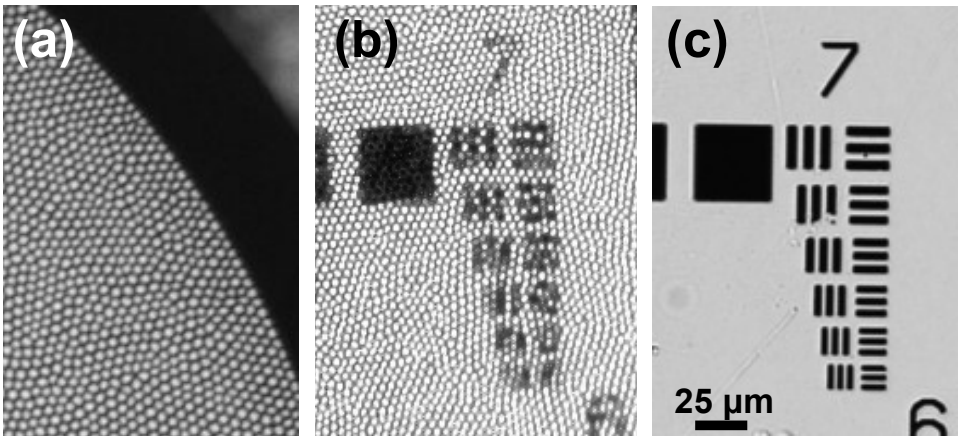

Figure 1. Limitations of fiber optic bundles. (a) Edge of a fiber bundle showing individually packed fibers. (b) Image of a USAF target viewed through a fiber bundle. Note the pixilation due to individual fibers and discontinuities due to inter-fiber "gaps". (c) Same area imaged with a benchtop microscope.

The past decade has seen a rise in "computational imaging" techniques that overcome some limitations of traditional imaging systems, including resolution and FOV[11–13]. While most imaging methods directly capture an image of the scene on a sensor, a computational imaging approach involves indirectly imaging the scene and employing computational techniques to provide novel functionality or improve imaging performance[14]. Such methods may also enable improved imaging performance when integrated in an endoscopic system. More specifically, techniques for compressive imaging (CI), a subset of computational imaging that refers to methods based on the signal processing field of compressed sensing (CS), have demonstrated the ability to reconstruct images with more resolvable pixels than are physically present in a sensor, allowing for high quality imaging in applications where sensor size is limited. Adapting these principles to fiber bundle imaging would potentially allow for endomicroscopy with resolution better than that defined by the fiber core spacing.

We propose using CI methods to resolve spatial detail *within* individual fibers of a bundle. We previously demonstrated that a CI architecture with coded masks placed at a conjugate image plane is a good candidate architecture for translation to fiber-bundle based endoscopy[15]. In this report we outline the mathematical model we developed for integrating a fiber bundle into an image-plane-coding CI system. We constructed a benchtop platform to test this model and we present preliminary results for CI through a fiber optic bundle. We conclude by identifying possible options for further improving this compressive endomicroscopy architecture.

2. METHODS

2.1 Compressive Imaging (CI)

CI is founded in the principles of compressed sensing (CS)[16–18] which state that a given signal can be accurately reconstructed with fewer samples, or measurements, than is typically expected using conventional sampling theory based on the Nyquist–Shannon theorem. CS theory specifies that it is possible to accurately reconstruct a discrete signal with a sampling rate that is less than twice the highest frequency of the signal, provided two requirements are met: (1) the discrete signal has high sparsity (many zero-valued elements) in some transform domain and (2) the domain that the signal is measured in is incoherent, or uncorrelated, with the domain where the signal is sparse[17]. Any photographed scene can be considered as a two- dimensional signal and it has been well documented that typical photographic data has high sparsity in, and is sufficiently uncorrelated with its representation in the wavelet domain[19].

CI generally requires acquisition of multiple sequential measurements, each capturing a differently modulated projection of the scene or sample. Spatial light modulators (SLM's) are typically used to impose a high spatial resolution amplitude and/or phase modulation onto light emanating from the scene, with multiple low-resolution measurements of this light recorded under different modulation patterns. Given these measurements (or "observations") and knowledge of the modulation, optimization-based CS algorithms are used to solve the inverse problem of recovering a high resolution image of the scene from the set of low resolution, modulated observations. Thus, CI makes it possible to reconstruct

images with resolution limited by the modulation pattern rather than the image sensor, allowing for high quality imaging in applications where sensor size is limited or high pixel densities are challenging or expensive to manufacture. Figure 2 illustrates the general CI process for an imaging sensor with orthogonally arranged square pixels. Here, a scene X' is modulated by a coded mask M_P containing m spatial elements. The modulated scene is then imaged onto a low-resolution sensor with n pixels, where $n < m$, capturing an observation, Y_P. Observations are captured for each of p different applied masks, generating p differently modulated images of the scene. CS reconstruction algorithms then use prior knowledge of the mask patterns to recover an image of the original scene X containing N pixels, where $n < N \leq m$. $N = m$ represents the highest resolution reconstruction, indicating that the system resolution is now theoretically limited by the mask rather than the sensor.

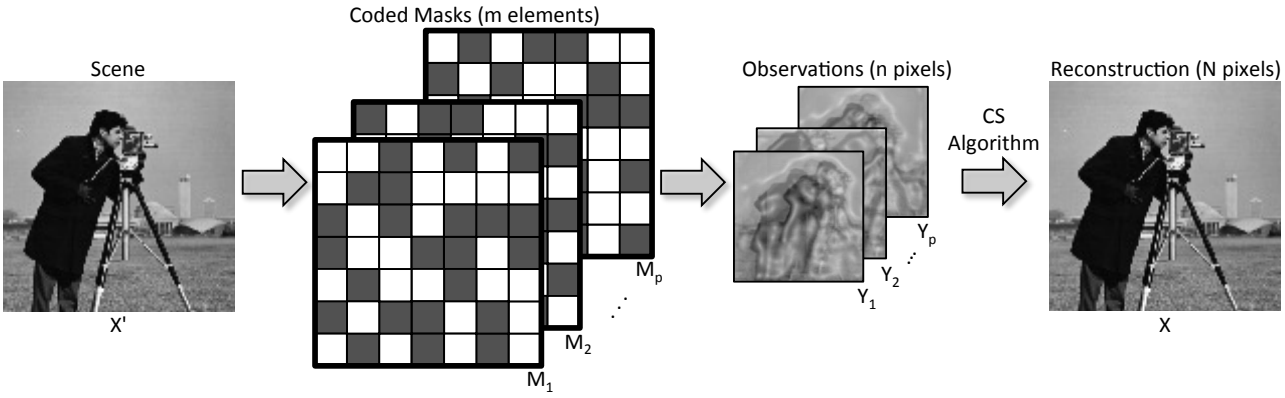

Figure 2. The general process for CI. A coded mask with m programmable elements modulates the scene, and an observation is captured by a low-resolution sensor with n pixels. After acquisition of p observations, each with a different (known) mask, CS algorithms solve the inverse problem to recover an image of the scene with N resolvable points.

Translating CI concepts to imaging through a fiber bundle requires additional details not illustrated in Figure 2. First, we consider the bundle as a low-resolution sensor array where each fiber transmits one value and can be considered a single pixel in the image. Second, while typical CMOS or CCD cameras have sensor arrays with square pixels arranged in an orthogonal pattern, the fiber cores in common bundles are circular and commonly arranged in a hexagonal pattern. Finally, a fiber-bundle-based imaging system requires additional optics and a camera to capture an image of the proximal face. Each of these details can be addressed by modifying the mathematical forward model for the system, as will be discussed in Section 2.3.

2.2 Mathematical Model

In a CI system without a fiber bundle, both the coded mask and sensor array have orthogonally arranged pixels and can be aligned such that an integer downsampling is maintained. We define the system's downsampling factor (d) as the square root of the number of mask elements that are imaged onto a single sensor pixel. Specifically, each $d \times d$ square block from the mask is geometrically mapped onto one pixel in the sensor array. In contrast, the individual fibers in the bundle are circular and roughly arranged in a hexagonal lattice. This mapping of square mask elements to circular fibers results in a non-uniform d, as some mask elements are only partially mapped onto the fibers. Additionally, the camera that images the proximal end of the bundle adds another level of sampling that must be addressed in image processing. The hexagonal organization of fibers creates blank areas (gaps) that are fixed for all observations. This can be considered as a secondary pattern F that can be included as a fixed term that is pointwise multiplied in the model. Also, an additional sampling factor D_f is included to define the imaging of fibers onto multiple sensor pixels at the proximal end. All pixels that are within the diameter of one fiber are effectively considered as one observation pixel by adding their individual values. The result is the following forward model for our fiber-bundle-based CI system:

$$Y_i = D_f \left\{ F \odot \left(D_r \left[H \otimes (M_i \odot X) \right] D_c \right) \right\} \tag{1}$$

Each applied mask (M_i) is pointwise multiplied with the object (X) and convolved with a system specific term H that accounts for optical imperfections, before two-dimensional downsampling (D_r, D_c) is applied (see *Dumas et al.*[20] for more details). We obtain F by uniformly illuminating the bundle and using a simple circle detection algorithm to distinguish inter-fiber regions from the fiber cores.

The general form of a traditional CS problem[17] can be written as $y = Ax$, where a vector representation of the object (x) is solved for, using the known measurement matrix (A) and vectorized measured observations (y). The components of the measurement matrix differ depending on the architecture used. Equation (1) can be modified for this vector representation as:

$$y_i = D_F T_f D T_H T_{M_i} X \tag{2}$$

where y_i is the $n^2 \times 1$ vectorized observation, x is the $m^2 \times 1$ vectorized object, T is a $m^2 \times m^2$ diagonal matrix with mask elements on the diagonal, T_H is a block Toeplitz convolution matrix obtained from H, and D denotes the appropriate downsampling operation (combining downsampling in both directions). T_f is a diagonal matrix with the entries of F on its diagonal. D_F is a binary {0, 1} matrix that defines the mapping of mask elements to the fibers in the bundle. The number of rows in D_F is equal to the number of fibers in the bundle and the number of non-zero entries in a row of D_F equals the number of mask elements mapped onto that respective fiber. Since the inter-fiber gaps are opaque, the information about regions of the object behind these gaps is lost and the algorithm can only recover details in the intra-fiber regions where there is observational data. All of this manipulation is done to bring the system into the recognized form, $y = Ax$, used in CS literature. Here $A = D_F T_f D T_H T_{Mi}$ denotes the measurement/sensing matrix, which is completely dependent on the system and highly impacts the quality of reconstructions (see *Dumas et al.*[21] for further details). In most cases, for computational imaging, one observation is insufficient to reconstruct x from y using CI reconstruction methods. Thus several observations are used, each with different masks, to obtain a larger system of equations that provides better reconstruction.

2.3 Experimental platform

Building on the architecture we have previously defined in *Dumas et al.*[15], we constructed a benchtop platform for CI in a fiber-bundle-based system. Specifically, a mask is included at a conjugate-image plane between the object and the distal end face of the bundle, with the proximal bundle face imaged onto a high-resolution CCD array (Figure 3(a)). The experimental benchtop platform we constructed (Figure 3(b)) uses a digital micromirror device (DMD) to simulate the projection of a "*synthetic object*" onto the mask. In this case, the mask is pointwise multiplied with the synthetic object image in software. In our hardware platform, projection optics consisting of two achromatic lenses image a 340×340 mirror region of the DMD (Texas Instruments LightCrafter EVM Module, 7.6 μm mirror pitch) onto the front end of a rigid fiber bundle (12.5 μm fiber core diameter) filling approximately 1,000 fiber cores in a central region of the bundle. The proximal end of the bundle is imaged onto a 340×340 pixel region of a CCD camera (Point Grey Research, GRAS-14S5M-C) via relay optics (two achromatic lenses). This arrangement results in an approximate downsampling factor of $d = 10.7$ as ~114 mirrors are imaged onto each fiber core. We previously found in software simulations of this architecture that a downsampling factor of $d = 5$ produces the best CI reconstructions (note the adjusted definition of d)[21]. To achieve this optimized downsampling, we use 2×2 binning of mask elements such that an effective mask element consists of four DMD mirrors. Results presented in the following section include CI reconstructions using masks with 4×4, 2×2, and no binning of DMD mirrors to evaluate how different values of d affect reconstruction quality.

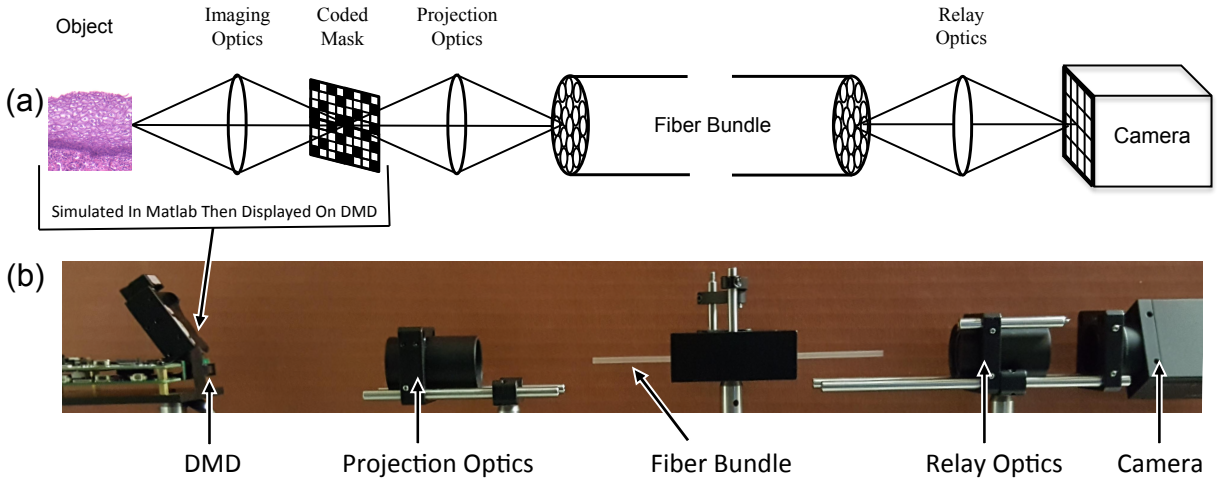

Figure 3. (a) Diagram of our compressive fiber bundle based endomicroscopy architecture. (b) Photograph of the experimental benchtop platform. DMD: Digital micromirror device.

3. RESULTS

Data was collected using the platform pictured in Figure 3(b) for synthetic objects. The image of a boat pictured in Figure 4(a) was displayed on the DMD and imaged using the camera at the proximal end of the fiber bundle. The resulting "no mask" image (Figure 4(b)) represents a conventional endoscope image where a snapshot of the object is taken with no intermediate mask. This shows substantial loss of detail when compared to the displayed object because each fiber transmits only a single value for all object detail imaged onto that fiber's diameter. CI results for undersampling factors of $d \approx 10.7$, 5.3, and 2.7 were evaluated using masks with 340×340 (Figure 4(c,d)), 170×170 (Figure 4(e,f)), and 85×85 (Figure 4(g,h)) elements, respectively (achieved through DMD binning). For all results the same 340×340 synthetic boat object was used and observations were captured through the fiber bundle with the same 340×340 pixel region on the DMD. Using CI with 100 observations through different masks (Figure 4(c,e,g), some of the fine details that were lost in with representative conventional endoscopy image (Figure 4(b)) are recovered, with qualitative assessment indicating that the set of 100 observations through 170×170 masks (Figure 4(e)) produces the best results. Specifically, some details within individual fibers are recovered, indicating that resolution is not limited by the fiber core spacing (e.g. see red arrows in Figure 4(e)). Ultimately, this CI arrangement could generate images with 170 × 170 = 28,900 resolvable points for a 1,000 fiber region of the bundle. For comparison, in conventional imaging each fiber acts as a single pixel which limits the number of resolvable points to 1,000 (i.e. the number of fiber cores). The CI reconstruction algorithm is restricted to reconstructing image data within the intra-fiber regions, so it does not recover any data from in the gaps. As a result, CI reconstructions still have the discontinuity inherent in fiber bundle imaging. To improve the visual appearance of the CI reconstruction, the gaps between fibers were filled in using bicubic interpolation, without affecting the intra-fiber values recovered with CI (Figure 4(d,f,h)). It should be noted that this method does not recover data from parts of the object that lie behind the intra-fiber gaps, but it does help visually discern features in the image.

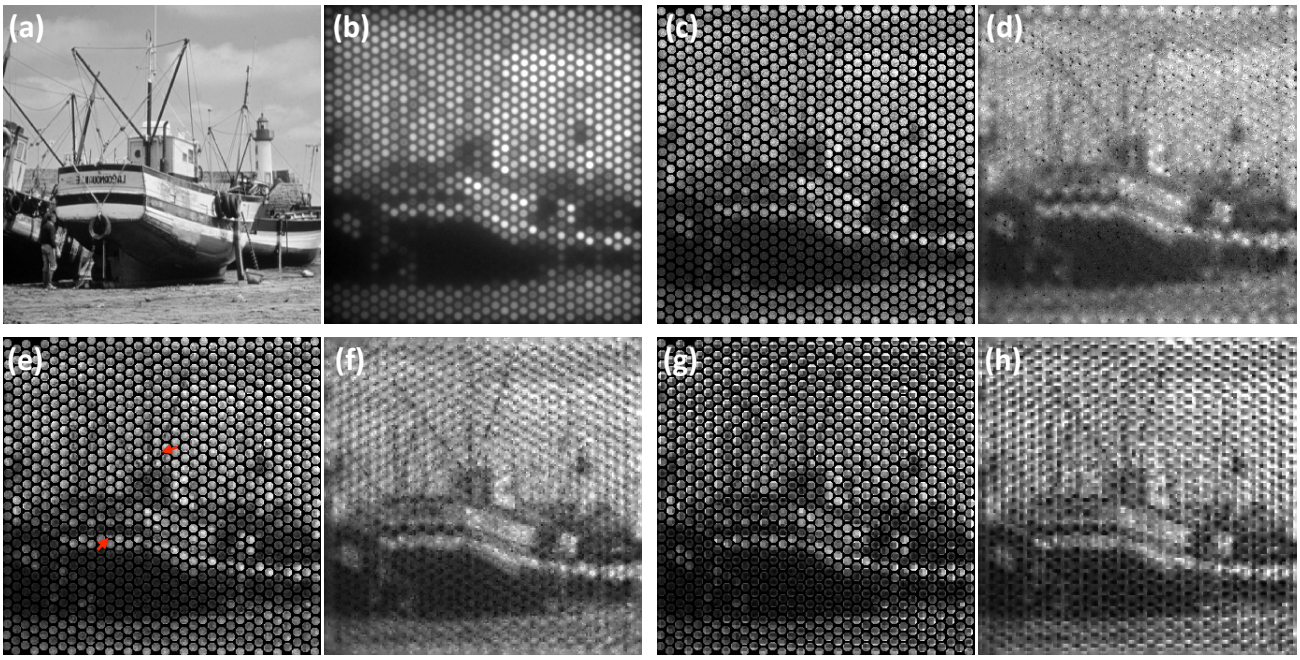

Figure 4. (a) Original synthetic boat image displayed on the DMD. (b) Image of the object with no intermediate mask representative of a conventional fiber bundle image. (c–h) CI reconstructions from 100 observations for (c) 340×340, (e) 170×170, and (g) 85×85 element masks and their results after interpolation to fill the gaps (d), (f), and (h), respectively

4. CONCLUSIONS

Based on qualitative assessment, images reconstructed using CI were able to resolve intra-fiber details that were not available when imaging through the fiber bundle alone, suggesting that more resolvable points can be recovered than

there are fiber cores in the imaging bundle. Furthermore, we found that the ratio of elements in the mask to fibers in the bundle, i.e. the downsampling factor, affects the quality of the final reconstructions. Specifically, a downsampling factor $d \approx 5.3$ of was found to generate the highest quality results in our CI platform, which is consistent with results from software simulations[21]. Since the resolution of this CI architecture is theoretically limited by the resolution of the mask rather than the resolution of the fiber bundle, it is expected that higher density masks with smaller elements will improve resolution further. While this is the case when comparing results for 85×85 masks with 170×170 masks, we found in this report, and in previous reports[15,20,21], that there is a limit to this relationship. Here, CI reconstructions using the denser 340×340 masks are of lower quality than the other reconstructions. This is likely due to a decrease in the diversity of observations acquired through different masks, which in turn makes the CS inverse problem more difficult to solve.

While the CS algorithms we used to generate images were restricted to reconstructing data within the intra-fiber regions, we found that simple post-processing with bicubic interpolation can substantially improve how the final image is perceived, by artificially filling in the inter-fiber gaps. Since this method does not actually regain details that lie behind the gaps, future work should be aimed at integrating this CI technique with other methods for eliminating pixilation artifacts in fiber-bundle-based endoscopes. Future goals involve evaluating other post-processing techniques such as matrix completion to improve reconstruction quality and investigating ways to integrate this CI approach with speckle correlation or image compounding approaches to simultaneously retrieve missing data due to inter-fiber gaps and resolve intra-fiber features. We believe this CI approach in conjunction with other endomicroscopy techniques can potentially meet the clinical demand for minimally-invasive endoscopes with sub-cellular spatial resolution and/or a wide FOV.

ACKNOWLEDGEMENTS

This research was funded by the NSF (CCF-1453073, ECCS- 1509260), and ARO (W911NF-14-1-0295).

REFERENCES

[1] Lee, C., and Han, J., "Elimination of honeycomb patterns in fiber bundle imaging by a superimposition method," *Opt. Let. 38*(12), 2023-2025 (2013).
[2] Kyrish, M., Kester, R., Richards-Kortum, R., & Tkaczyk, T., "Improving spatial resolution of a fiber bundle optical biopsy system," Proc. SPIE 7558, 755807 (2010).
[3] Bedard, N., and Tkaczyk, T. S., "Snapshot spectrally encoded fluorescence imaging through a fiber bundle," J. Biomed. Opt. 17(8), 0805081-0805083 (2012).
[4] Cheon, G. W., Cha, J., and Kang, J. U., "Random transverse motion-induced spatial compounding for fiber bundle imaging," Opt. Let. 39(15), 4368-4371 (2014).
[5] Kim, D., Moon, J., Kim, M., Yang, T. D., Kim, J., Chung, E., and Choi, W., "Toward a miniature endomicroscope: pixelation-free and diffraction-limited imaging through a fiber bundle," Opt. Let. 39(7), 1921-1924 (2014).
[6] Čižmár, T., and Dholakia, K., "Exploiting multimode waveguides for pure fibre-based imaging," Nature communications 3, 1027 (2012).
[7] Mahalati, R. N., Gu, R. Y., and Kahn, J. M., "Resolution limits for imaging through multi-mode fiber," Opt. Express 21(2), 1656-1668 (2013).
[8] Stasio, N., Moser, C., and Psaltis, D., "Calibration-free imaging through a multicore fiber using speckle scanning microscopy," Opt. let. 41(13), 3078-3081 (2016).
[9] Sivankutty, S., Tsvirkun, V., Bouwmans, G., Kogan, D., Oron, D., Andresen, E. R., and Rigneault, H., "Extended field-of-view in a lensless endoscope using an aperiodic multicore fiber," Opt. Let., 41(15), 3531-3534 (2016).
[10] Shin, J., Bosworth, B. T., & Foster, M. A., "Compressive fluorescence imaging using a multi-core fiber and spatially dependent scattering," Opt. Let. 42(1), 109-112 (2017).
[11] Stern, A., "Optical compressive imaging and sensing: A decade retrospective," IEEE Information Optics (WIO), 2016 15th Workshop, 1-3 (2016).
[12] McLeod, E., and Ozcan, A., "Unconventional methods of imaging: computational microscopy and compact implementations," Reports on Progress in Physics, 79(7), 076001 (2016).
[13] Arce, G. R., Brady, D. J., Carin, L., Arguello, H., and Kittle, D. S., "Compressive coded aperture spectral imaging: An introduction," IEEE Signal Processing Magazine 31(1), 105-115 (2014).

[14] Cossairt, O., Gupta, M., and Nayar, S. K., “When does computational imaging improve performance?” IEEE transactions on image processing, 22(2), 447-458 (2013).
[15] Dumas, J. P., Lodhi, M. A., Bajwa, W. U., and Pierce, M. C., “From modeling to hardware: an experimental evaluation of image plane and Fourier plane coded compressive optical imaging,” Opt. Express 25(23), 29472-29491 (2017).
[16] Donoho, D. L., “Compressed sensing,” IEEE Transactions on information theory, 52(4), 1289-1306 (2006).
[17] Baraniuk, R. G., “Compressive sensing,” IEEE signal processing magazine 24(4), 118-121 (2007).
[18] Candès, E. J., Romberg, J., and Tao, T., “Robust uncertainty principles: Exact signal reconstruction from highly incomplete frequency information,” IEEE Transactions on information theory, 52(2), 489-509 (2006).
[19] Daubechies, I., “Ten lectures on wavelets,” SIAM 62, (1992).
[20] Dumas, J. P., Lodhi, M. A., Bajwa, W. U., and Pierce, M. C., “Computational imaging with a highly parallel image-plane-coded architecture: challenges and solutions,” Opt. Express 24(6), 6145-6155 (2016).
[21] Lodhi, M. A., Dumas, J. P., Pierce, M. C. and Bajwa, W. U., "Computational imaging through a fiber-optic bundle." International Society for Optics and Photonics Proc. Compressive Sensing VI: From Diverse Modalities to Big Data Analytics 10211, 1021108 (2017).